EPJ Web of Conferences **45**, 01071 (2013)
DOI: 10.1051/epjconf/20134501071

Effect of High Porosity Screen on the Near Wake of a Circular Cylinder

G.M. Ozkan[1, a], H. Akilli[1], and B. Sahin[1]

[1] Faculty of Engineering and Architecture, Department of Mechanical Engineering, Çukurova University, 01330, Adana, Turkey

Abstract. The change in flow characteristics downstream of a circular cylinder (inner cylinder) surrounded by a permeable cylinder (outer cylinder) made of a high porosity screen was investigated in shallow water using Particle Image Velocimetry (PIV) technique. The diameter of the inner cylinder, outer cylinder and the water height were kept constant during the experiments as d = 50 mm, D = 100 mm and h_w = 50 mm, respectively. The depth-averaged free stream velocity was also kept constant as U = 180 mm/s which corresponded to a Reynolds number of Re_d = 9000 based on the inner cylinder diameter. It was shown that the outer permeable cylinder had a substantial effect on the vortex formation and consequent vortex shedding downstream of the circular cylinder, especially in the near wake. The time averaged vorticity layers, streamlines and velocity vector field depict that the location of the interaction of vortices considerably changed by the presence of the outer cylinder. Turbulent statistics clearly demonstrated that in comparison to the natural cylinder, turbulent kinetic energy and Reynolds stresses decreased remarkably downstream of the inner cylinder. Moreover, spectra of streamwise velocity fluctuations showed that the vortex shedding frequency significantly reduced compared to the natural cylinder case.

1 Introduction

The phenomenon of Vortex Induced Vibration (VIV) around bluff bodies is of practical interest of many fields in engineering since its outputs have several undesirable effects such as structural vibrations, increase in drag and lift forces on the body. If the frequency of VIV approaches to the natural frequency of bluff body, the case of resonance takes place and consequently sudden structural failures may occur. VIV is caused by the unsteady vortex shedding which results in a pressure difference between the leading and trailing edges of the body, so the net drag force exerted on the body also increases. Although being an advantage for heat exchanger tubes, VIV is a serious problem in many engineering applications such as bridges, high-rise buildings, chimneys, turbine blades, cooling systems for nuclear power plants, power transmission lines etc. In recent years investigations have been focused on applications in offshore engineering since oil risers (steel pipes) are being broken like a wire by large amplitude VIV's caused by the deep ocean currents. Ocean engineers are being busy with solving this problem because riser systems cost one-third of an entire offshore production unit. Therefore, the effective control of vortex induced vibrations is essential in these types of engineering applications.

Flow control can principally be achieved by controlling the separation of the boundary layer and various possible methods have been applied towards this aim, such as suction, blowing, surface roughness elements and splitter plate, etc. Therefore, many studies have been carried out in the past [1, 2, 3, 5, 6, 7, 9, 10, 12, 13, 14, 16] to establish a method to control the vortex shedding which can be observed easily when fluid flows over a bluff body. A classification may be done by dividing the control methods into two categories, namely passive and active flow control. Passive control techniques modify a flow without external energy expenditure whereas active control ones apply some sorts of energy into the flow. As can be expected, passive control methods are cheaper and more applicable on the systems compared to other methods.

There are numerous investigations in the literature based on active and passive flow control. A good review by Choi et al. [4] presents control methods for flow over a bluff body such as a circular cylinder, a 2D bluff body with a blunt trailing edge, and a sphere. They introduced recent major achievements in bluff- body based flow controls such as 3D forcing, active feedback control, control based on local and global instability, and control with a synthetic jet. They also classified the controls as boundary-layer controls and direct-wake modifications and discuss important features associated with these

[a] gmozkan@cu.edu.tr

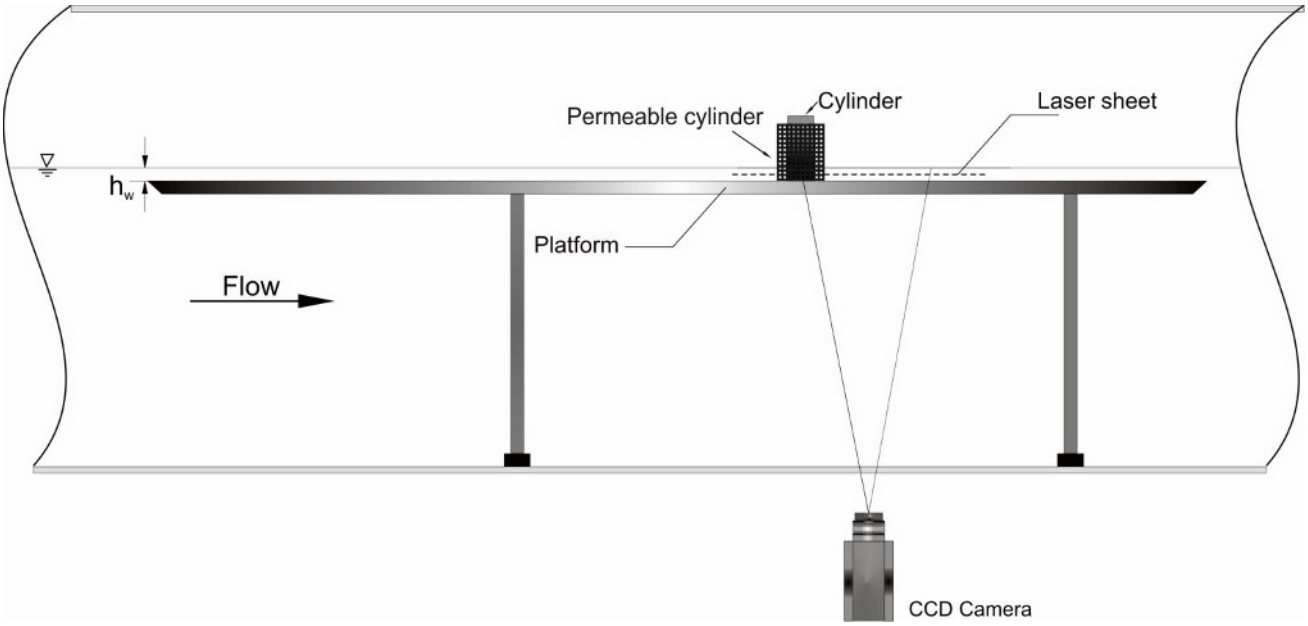

Fig. 1. Side view of the experimental set-up

controls. Kumar et al. [8] presented a review of the passive control of VIV through various means particularly emphasizing some recent inventions patented in this area. Their review indicates that, in practical applications especially in marine engineering situations, passive control measures such as employing a streamline fairing or a helical strake prolong the life of offshore structures by protecting them from vortex-induced vibrations. Their study also includes recent patents on this topic and concludes with a note on the current and future developments expected in the passive control of VIV.

In this study, control of the flow around a circular cylinder was attempted by perturbing its near wake with a surrounding outer permeable cylinder.

2 Experimental Method

Experiments were carried out in a circulating open water channel having dimensions of 8000 mm × 1000 mm × 750 mm located at Fluid Mechanics Laboratory of Mechanical Engineering Department of Çukurova University. The PIV technique was utilized to determine both instantaneous and the time-averaged velocity vector fields downstream of a vertical cylinder with a diameter of d = 50 mm in order to see the effect of the control element which is concentrically located as an outer cylinder made of a chrome-nickel wire mesh to control the vortex shedding behavior in shallow water flow. Streamline topology, instantaneous and mean vorticity maps have been acquired by post-processing as well as Reynolds stress correlations. Side view of the experimental set-up, position of the cylinder, the laser sheet's location and the view of camera are shown in figure 1. The total depth of the water in the channel was set at 600 mm. All experiments were conducted above a platform having a length of 2300 mm as shown in figure 1. The distance between the leading edge of the platform and the cylinder was 1800 mm to obtain fully developed boundary layer. The water height between the base of the platform and the free surface was adjusted to 50 mm. The ratio between the inner cylinder diameter and the width of the test section, geometric blockage of the inner cylinder, was 5%. According to the permeable outer cylinder, geometric blockage ratio increases up to 10%. In order to prevent wall effects, the blockage ratio was kept constant as 10% [15], resulting in a maximum outer permeable cylinder diameter of 100mm (D/d = 2.0).The flow of the water inside the channel was achieved using a pump driven by an electric motor having a variable speed controller. Depth-averaged velocity was U=180 mm/s corresponding to the Reynolds number of Re=9000 based on the cylinder diameter and Froude number of Fr = 0.257 based on the water depth.

Figure 2 shows the schematic representation of the dimensions of inner cylinder diameter (d), outer cylinder diameter (D), mesh size (a) and mesh diameter (t) as well as the reference coordinate system and a formulation for the definition of porosity (the ratio of the gap area on the body to the whole body surface area), β. Outer cylinder of 100 mm diameter and the porosity of $\beta = 0.7$ was used for controlling vortex shedding downstream of the circular cylinder. The control element (outer cylinder) was placed concentrically with the reference cylinder of 50 mm.

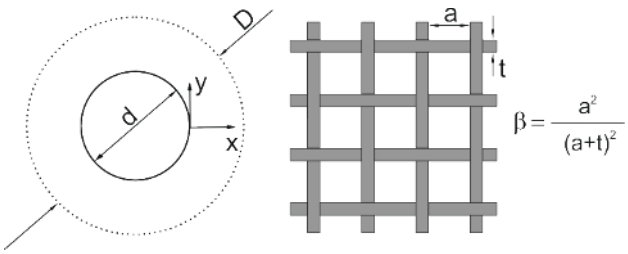

Fig. 2. Schematic representation for the dimensions of inner cylinder, permeable outer cylinder as well as the reference coordinate system, definition for the porosity, β

The experimental data was acquired and processed using Dantec Dynamics PIV system and Flow Manager software installed on a computer. The measurement field was illuminated by a thin and intense laser light sheet by using a pair of double-pulsed Nd:YAG laser units each having a maximum energy output of 120 mJ at 532 nm wavelength. The laser sheet was oriented parallel to the bottom surface of the water channel and the experiments were carried out at the midplane of the water height. The image capturing was performed by an 8 bit cross-correlation charge-coupled device (CCD) camera having a resolution of 1600 pixels x 1200 pixels, equipped with a Nikon AF Micro 60 f / 2.8D lens. In the image processing, 32x32 rectangular interrogation pixels were used and an overlap of 50% was employed. The total 7227 (99 × 73) velocity vectors were obtained for an instantaneous velocity field at a rate of 15 frames/s. The overall view field was taken as 160 mm x120 mm in physical size in order to have detailed and accurate results about the flow structure in the wake of the inner cylinder. The time interval between pulses was 1.75 ms and the thickness of the laser sheet illuminating the measuring plane was nearly 2 mm throughout the experiments. The values of time interval and the laser sheet thickness were selected to achieve the maximum amount of particles in the interrogation window. The uncertainty in velocity relative to depth-averaged velocity is about 2% in the present experiments. The water was seeded with 12 μm diameter hollow glass sphere particles having a density of 1100 kg / m^3. In each experiment, 350 instantaneous images were captured and recorded in order to have the time-averaged velocity vector field and other flow characteristics. Spurious velocity vectors (less than 2%) were omitted using the local median-filter technique and replaced by using a bilinear least squares fit technique between surrounding vectors. Furthermore, the velocity vector field was smoothed by using the Gaussian smoothing technique to avoid dramatic changes in the velocity field. The vorticity value at each grid point was computed from the circulation around the eight neighboring points.

3 Results and Discussion

Figure 3 illustrates the patterns of time-averaged streamline topology, <Ψ> and velocity vector field, **<U>**. It is clearly seen from the figure that the time-averaged flow characteristics are almost symmetrical with respect to the centerline. First column of the figure demonstrates the results of the natural cylinder where two well-defined foci designated by F_1 and F_2 and a saddle point, S are formed downstream of the cylinder. Accordingly, a recirculation region exists in the wake of the cylinder in alignment with the location of the foci. Magnitudes of the velocity vectors increase along the shear layer of the cylinder and lose their strength in further downstream locations. Second column of the figure 3 presents the controlled case where the outer permeable cylinder significantly affects the flow structure downstream of the inner cylinder. As seen from the streamlines, the foci, F_1 and F_2 get closer to the rearward stagnation point of the inner cylinder and formed in between the inner and outer cylinder. However, the saddle point, S retreats upstream and formed at a location very close to the rearward stagnation point of the outer cylinder. The velocity vector field of the inner-outer cylinder arrangement (controlled case) clearly demonstrates that the recirculation of vortices gets closer to the back stagnation point of the inner cylinder. However, the magnitude of velocity vectors gets smaller in the downstream region compared to the natural cylinder case.

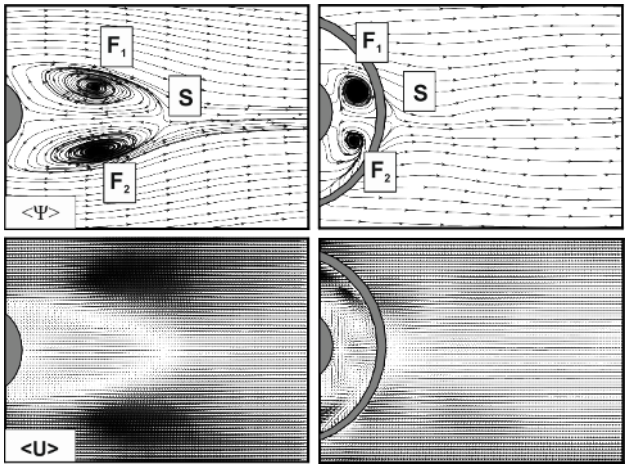

Fig. 3. The patterns of time-averaged streamline topology, **<Ψ>** and velocity vector field, **<U>** for natural cylinder and the inner-outer cylinder arrangement

Figure 4 presents the contours of time-averaged vorticity, <w>, Reynolds shear stress, <u`v`>, and turbulent kinetic energy for the natural cylinder and the inner-outer cylinder arrangement. The solid and dashed lines present positive (counterclockwise) and negative (clockwise) contours, respectively. First row of the figure 4 shows the mean vorticity contours where the minimum and incremental values are ±5 and 5, respectively. The contours of the time-averaged vorticity are symmetrical and get closer to each other in further downstream locations for the natural cylinder case. For the controlled case, the outer cylinder enforces the vortices to be formed in between the inner and outer cylinder and the maximum value of the vorticity decreases by 49% compared to the natural cylinder case. Besides, the vortices get close to each other just behind the back stagnation point of the inner cylinder which is an indication of interaction between upper and lower vortices. Furthermore, it is obvious that the vorticity layers formed by the inner cylinder cannot be seen anymore along the downstream of the outer cylinder; however the small magnitude vorticity layers exist along the shear layers of the outer cylinder. So, it can be concluded that vorticity layers downstream of the inner cylinder are suppressed by the outer permeable cylinder. Second row of the figure 4 shows the Reynolds shear stress correlations where the minimum and incremental values are ±0.13 and 0.005, respectively for the natural cylinder and ±0.05 and 0.005, respectively for the controlled case. First of all, it is clearly seen that the clusters of Reynolds shear stress contours are almost symmetrical with respect to the

centerline for both natural and controlled cases. The peak value of the normalized Reynolds shear stress is 0.129 for the natural cylinder case as seen in the figure. When the outer cylinder takes place, this peak dramatically decreases to a value of 0.036 which correspond to a 72% reduction. The Reynolds shear stress plays a dominant role in the theory of mean momentum transfer by turbulent motion [11]. Therefore, the reduction in the Reynolds shear stress by existence of an outer permeable cylinder results in weakening of the vortex shedding downstream of the inner cylinder. The spatial distribution of turbulent kinetic energy (TKE) shown in the third row of figure 4 provides distinct information about the turbulence intensity of the flow field. The maximum value of TKE for the natural cylinder case increases initially in the downstream direction starting from the base of the cylinder and reach its peak value of 0.28 at a position near the saddle point, S. Then, it starts to dissipate gradually in the downstream flow direction. For the controlled case, it is clearly seen from the figure that the outer cylinder has a dramatic effect on the concentrations. The maximum value of TKE occurs close to the back stagnation point of the outer cylinder with a value of 0.108 which corresponds to a reduction of 61.4% in intensity. This high amount of reduction in turbulent kinetic energy means that fluctuations in both streamwise and transverse flow directions are attenuated by the outer permeable cylinder; consequently the momentum of flow is also reduced resulting in lower momentum transfer from the free stream into the wake region.

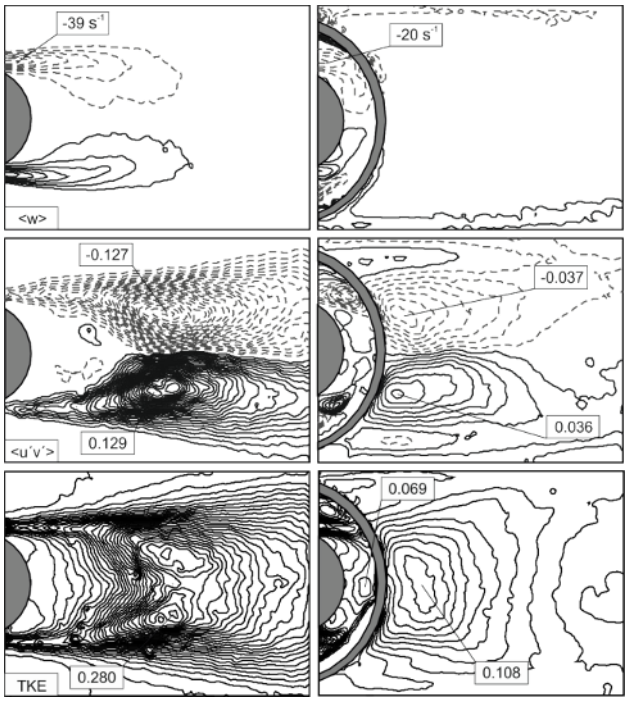

Fig. 4. The contours of time-averaged vorticity, <w>, Reynolds shear stress, <u`v`>, and turbulent kinetic energy for both cases

Figure 5a and 5b demonstrates the spectra of streamwise velocity fluctuations for the natural cylinder case and the inner-outer cylinder arrangement, respectively. A distinct peak with f = 0.705 at the streamwise location of x/d = 1.8 is obviously seen in figure 5a which is an indication of a dominant vortex structure resulting in periodic vortex shedding downstream of the cylinder. This frequency value of f = 0.705 corresponds to a Strouhal number of St = 0.2 ($St = f/U$) which is in good agreement with the literature.

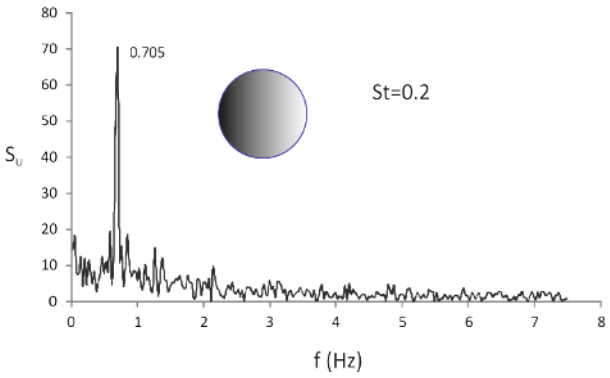

Fig. 5a. The power spectra of streamwise velocity fluctuations for the natural cylinder

As mentioned in the previous results, the outer cylinder has significant impact on the flow structure of the inner cylinder; therefore it is also supposed that the frequency of the vortex shedding might be affected, too. In figure 5b, the points 1, 2, 3 and 4 correspond to the streamwise locations of x/d = 0.3, 1.0, 1.4 and 1.8, respectively. The results of point 1, located between the inner and outer cylinder shows a distinct peak with a frequency of f = 0.411. It is previously known from the natural cylinder case that this frequency corresponds to a dominant vortex structure and consequent vortex shedding even for the controlled case. However, the frequency of inner-outer cylinder arrangement results in a Strouhal number of St = 0.11 which is 45% lower compared to the natural cylinder case. Besides, frequencies obtained on the points 2, 3 and 4 shows that the amplitude of this dominant peak diminishes along the downstream of the outer cylinder maintaining the value of f = 0.411.

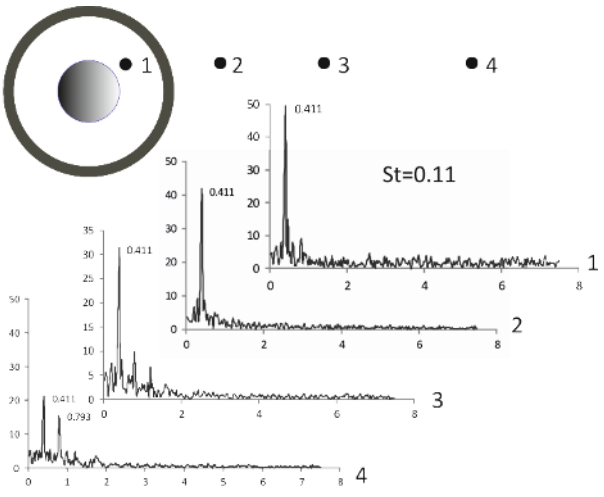

Fig. 5b. The power spectra of streamwise velocity fluctuations for the inner-outer cylinder arrangement

So, it can be concluded that the vortex shedding from the inner cylinder is not completely eliminated by the outer cylinder, however the frequency of the vortex shedding is remarkably reduced compared to the natural case which might be important in some practical applications where high-frequency vortices have harmful effects on the structures such as bridge piers, high-rise chimneys, risers in offshore engineering, etc.

.4 Conclusions

Flow structure of a circular cylinder (inner cylinder) surrounded by an outer permeable cylinder is investigated experimentally by using Particle Image Velocimetry (PIV) technique in shallow water flow. The organized vortex structure from the inner cylinder is perturbed by an outer permeable cylinder having a porosity of $\beta = 0.7$. Experiments showed that existence of an outer permeable cylinder considerably modifies streamline topologies and the velocity vector fields of the inner cylinder. The turbulent statistics obtained from PIV measurements have indicated that the peak magnitudes of turbulent kinetic energy and Reynolds shear stresses decrease remarkably due to the presence of the outer cylinder. Furthermore, spectra of streamwise velocity fluctuations revealed that the vortex shedding frequency is considerably reduced which might be helpful for many practical applications. Further studies including lift and drag measurements would be helpful for better understanding the effect of an outer permeable cylinder on the flow control around bluff bodies.

References

1. H. Akilli, B. Sahin, N.F. Tumen, Flow. Meas. Instrum. **16**, 211 (2005)
2. H. Akilli, C. Karakus, A. Akar, B . Sahin, N.F. Tumen, J. Fluid Eng.-T ASME **130**, 1, (2008)
3. H. Baek, G.E. Karniadakis, J. Fluid. Struct. **25**, 848, (2009)
4. H. Choi, W. Jeon, J. Kim, Annu. Rev. Fluid. Mech. **40**, 113, (2008)
5. B.G. Dehkordi, H.H. Jafari, J. Fluid. Eng-T ASME, **132**:044501,(2010)
6. K. Kwon, H. Choi, Phys. Fluids **8**, 479, (1996)
7. C.H. Kuo, L.C. Chiou, C.C. Chen, J. Fluid. Struct. **23,** 938, (2007)
8. R.A. Kumar, C-H. Sohn and B.H.L Gowda, Recent Patents on Mechanical Engineering, **1**, 1,(2008)
9. S. Mittal, A. Raghuvanshi, Int. J. Num. Meth. Fl. **35**, 421, (2001)
10. Rathakrishnan, AIAA J. **37**, 1125, (1999)
11. H. Tennekes, J.L. Lumney, *A first course in turbulence, 3rd edn.* The MIT Press, Cambridge, MA, (1974)
12. S. Turki, Eng. Appl. Comput. Fluid Mech., **2**:514, (2008)
13. M.F. Unal, D. Rockwell, J. Fluid Mech. **190,** 513, (1988)
14. J.J. Wang, P.F. Zhang, S.F. Lu, K. Wu, Flow. Turbul. Combust. **76**, 83, (2006)
15. G.S. West, C.J. Apelt, J. Fluid Mech., **114,** 361, (1981)
16. S.B. Yucel, O. Cetiner, M.F. Unal, Exp. Fluids **49**, 241, (2010)